SCIENTIFIC REPORTS
nature research

OPEN

Epoxy pre-polymers as new and effective materials for corrosion inhibition of carbon steel in acidic medium: Computational and experimental studies

Received: 1 April 2019
Accepted: 1 August 2019
Published online: 12 August 2019

Omar Dagdag[1], Zaki Safi[2], Rachid Hsissou[1], Hamid Erramli[3], Mehdi El Bouchti[4], Nuha Wazzan[5], Lei Guo[6], Chandrabhan Verma[7,8], E. E. Ebenso[7,8] & Ahmed El Harfi[1]

Present study is designed for the synthesis, characterization and corrosion inhibition behavior of two diamine aromatic epoxy pre-polymers (DAEPs) namely, N^1,N^1,N^2,N^2-tetrakis (oxiran-2-ylmethyl) benzene-1,2-diamine (DAEP1) and 4-methyl-N^1,N^1,N^2,N^2-tetrakis (oxiran-2-ylmethyl) benzene-1,2-diamine (DAEP2) for carbon steel corrosion in acidic medium. Synthesized DAEPs were characterized using spectral (Nuclear magnetic resonance (^{1}H NMR) and Fourier transform infrared-attenuated total reflection (FTIR-ATR)) techniques. Viscosity studies carried out at four different temperatures (20–80 °C) increase in temperature causes significant reduction in their viscosities. The anticorrosive properties of DAEPs differing in the nature of substituents, for carbon steel corrosion in 1 M HCl solution was evaluated using several experimental and computational techniques. Both experimental and computational studies showed that inhibitor (DAEP2) that contains electron releasing methyl (-CH_3) showed higher protectiveness as compared to the inhibitor (DAEP1) without substituent (-H). Electrochemical results demonstrate that DAEPs act as reasonably good inhibitors for carbon steel in 1 M HCl medium and their effectiveness followed the sequence: DAEP2 (92.9%) > DAEP1 (91.7%). The PDP results show that the diamine aromatic epoxy pre-polymers molecules (DAEPs) act as mixed type inhibitors. Electrochemical study was also supported using scanning electron microscopy (SEM) method were significant improvement in the surface morphology of inhibited (by DAEPs) metallic specimens was obtained. Results derived from computational density functional theory (DFT) and molecular dynamics (MD) simulationsand studies were consistent with the experimental results derived from SEM, EIS and PDP electrochemical studies. Adsorption of the DAEPs obeyed the Langmuir adsorption isotherm model.

Corrosion of steel alloys is one of the most important safety and economic anxiety for many industries including oil-gas and petroleum industries. Carbon steel is one of the frequently used steel based materials for numerous

[1]Laboratory of Agroresources, Polymers and Process Engineering (LAPPE), Department of Chemistry, Faculty of Science, Ibn Tofail University, BP 133, 14000, Kenitra, Morocco. [2]Al Azhar University-Gaza, Chemistry Department, Faculty of Science, P.O Box 1277, Gaza, Palestine. [3]Laboratory of Materials, Electrochemistry and Environment, Department of Chemistry, Faculty of Sciences, Ibn Tofail University, Kenitra, Morocco. [4]Higher School of Textile and Clothing Industries, Laboratory REMTEX, BP 7731, Oulfa, Casablanca, Morocco. [5]King Abdulaziz University, Chemistry Department, Faculty of Science, P.O Box 42805, Jeddah, 21589, Saudi Arabia. [6]School of Materials and Chemical Engineering, Tongren University, Tongren, 554300, China. [7]Material Science Innovation & Modelling (MaSIM) Research Focus Area, Faculty of Natural and Agricultural Sciences, North-West University, Private Bag X2046, Mmabatho, 2735, South Africa. [8]Department of Chemistry, Faculty of Natural and Agricultural Sciences, School of Chemical and Physical Sciences, North-West University, Private Bag X2046, Mmabatho, 2735, South Africa. Correspondence and requests for materials should be addressed to C.V. (email: chandraverma.rs.apc@itbhu.ac.in) or E.E.E. (email: Eno.Ebenso@nwu.ac.za)

many applications in several industries because of its excellent mechanical power and relatively low cost. However, it is highly susceptible to corrosion during several industrial processes where metallic components undergo corrosive dissolution by aggressive acidic attack. Hydrochloric acid is one of the most utterly used acids for these processes due to the fact of its relatively low cost, aggressive nature, efficiency in comparison to other mineral acids. However, the continuous utilization of acids in these repetitive processes may induce corrosion of steel materials and then deterioration of the industrial tools[1–3]. The addition of corrosion inhibitor into the acid is used to reduce the corrosive attack of acid by adsorbing themselves onto the steel surface and prevents the direct contact of acid with the casing and tubing steel[4,5]. The corrosion inhibitors can adsorb at the interfaces of metals and electrolytes and form protective surface covering with the aid of polar functional groups constituted by heteroatoms (N, P, O, and S) as well as through the π-electrons of functional groups and aromatic rings. Among the inhibitors which are effective in acid solutions there are nitrogen containing compounds (amines, amides, diamines)[6–10]. The computational studies present informations in relation to the effectiveness of the metal-inhibitor interactions along with the orientation of the inhibitor molecule(s) on the metallic surface. Employment of the DFT in corrosion inhibition of metallic surface in acidic medium in the presence of organic inhibitors is also gaining recent attention. With DFT-based studies, it became promising to gain detail about the organic film electronic features prevailing its adhesion manner with regards to substrate[11–15]. Apart from DFT study, computational study being carried out using MD simulations give some useful parameters through which metal-inhibitor(s) interactions and orientation of the inhibitors at meta-electrolyte interface can be derived[16,17].

Epoxy pre-polymers are multifunctional macromolecular matrices that are widely used in large amounts as heavy-duty anticorrosion coatings due to its outstanding adhesion to many substrates, high strength, corrosion resistances and excellent chemical resistance properties[18,19]. Novelty of the present study lying on the fact that DAEPs are used as corrosion inhibitors for the first time therefore use of this type of compounds as corrosion inhibitors should be explored. Outcome of the study suggested that inhibitor containing methyl substituent showed higher effectiveness than the inhibitor without any substituent. Therefore, present study will help in the designing of the effective corrosion inhibitors for future studies. The selection of diamine aromatic epoxy pre-polymers (DAEPs) as corrosion inhibitors in present investigation is also based on the facts that they are associated extensive conjugation in the form of multiple (double) bonds of aromatic rings and non-bonding electrons of heteroatoms (oxygen and nitrogen) that can offer strong interactions with the metallic surface. Further, DAEPs are also associated with highly reactive four epoxy rings in their molecular structures that easily undergoes acid catalyzed ring opening reaction and get converted into hydroxyl group (-OH) that can further enhance their adsorption ability on metallic surface as well as solubility in the polar electrolytic medium of 1 M HCl. In present study, we synthesized, characterized and demonstrated the anticorrosive property the two diamine aromatic epoxy pre-polymers (DAEPs) namely,N^1,N^1,N^2,N^2-tetrakis (oxiran-2-ylmethyl) benzene-1,2-diamine (DAEP1) and 4-methyl-N^1,N^1,N^2,N^2-tetrakis (oxiran-2-ylmethyl) benzene-1,2-diamine (DAEP2) on carbon steel corrosion in acidic medium. In the first part of our present study, we demonstrated the viscosity and viscoelastic measurements of both the investigated (DAEPs) molecules and outcomes of the study showed DAEPs at 20 °C behave as Newtonian liquids and heightening of the temperature reduced their viscosity. Numerous viscoelastic properties including storage modulus (G'), loss modulus (G'') and complex viscosity (η^*) as a function of angular frequency at different temperatures (20–60 °C) is also evaluated. Both DAEPs are evaluated for their anticorrosive behavior on carbon steel corrosion in 1 M HCl solution using PDP, EIS, SEM, DFT and MD methods. More so, diamine aromatic epoxy pre-polymers contain several electron rich sites in the form of atoms other than carbon (N and O) and π-electrons by way of which they can adsorb effectually and obstruct corrosion thereafter. Both investigated compounds act as good corrosion inhibitors. Thermodynamic parameters for the steel corrosion in 1 M HCl solution with and without diamine aromatic epoxy pre-polymer DAEP2 at its 10^{-3} M concentration were evaluated at various temperatures (298–328 K). The adsorption and inhibition behavior of diamine aromatic epoxy pre-polymers DAEPs were supported by DFT and MD computational techniques.

Experimental

Materials. The chemicals and materials used in this work such as 1,2-Diaminobenzene (≥99%), 4-Methyl-1,2-phenylenediamine (≥98%), epichlorohydrin (99%) and triethylamine (≥99.5%) were purchased from Aldrich chemical company. Steel alloy having composition described in our previous study[20–22] were used as working (test) material. Preparation of the electrolyte and metallic specimens can be found elsewhere[23]. The DAEPs was synthesized by the reaction of diamine with epichlorohydrin in the presence of triethylamine (NEt_3) as per the course of action reported in the literature[24,25]. Schematic diagram for the preparation of the diamine aromatic epoxy pre-polymers (DAEPs) is shown in Fig. 1. Informations related to the synthesized DAEP sare given in Figs SI1 and SI2 and Table SI2. In brief, aromatic diamines (10^{-2} mol) were dissolved and in 10 mL of ethanol (10 mL) in two-neckRB flask. In the above reaction mixture, 2.5 mL of epichlorohydrin (2.5 mL) was added slowly with continuous stirring. Resultant mixture was allowed to worm around 70 °C for 4 h. The resultant reaction mixture was again allowed to stir at 40 °C for 3 h, after the addition of 3 mL of triethylamine (NEt_3). Viscous solution of desired resins was obtained by evaporating residual solvents using a rotary evaporator. Synthesized inhibitors were characterized using spectral techniques. Infrared (IR) spectra were registered with a Bruker Fourier transform infrared (FTIR) using the FT-IR-attenuated total reflection technique. Following parameters were used: resolution 4 cm^{-1}, spectral range 500–4000 cm^{-1}, number of scans 128. ^{1}H NMR spectra were recorded on a Bruker AVANCE 300 MHz instrument with DMSO-d_6 as solvent and $(CH_3)_4Si$ as an internal standard. All ^{1}H-NMR experiments are reported in δ units.

Viscosity and viscoelastic measurements. The viscosity and viscoelastic measurements of the two synthesized DAEPs were studied using Haake Mars rheometer having 25 mm diameter parallel plate geometry with a 0.5 mm gap. The viscosity measurements were carried out at a shear rate ranged between 0.01 and 150 s^{-1} at

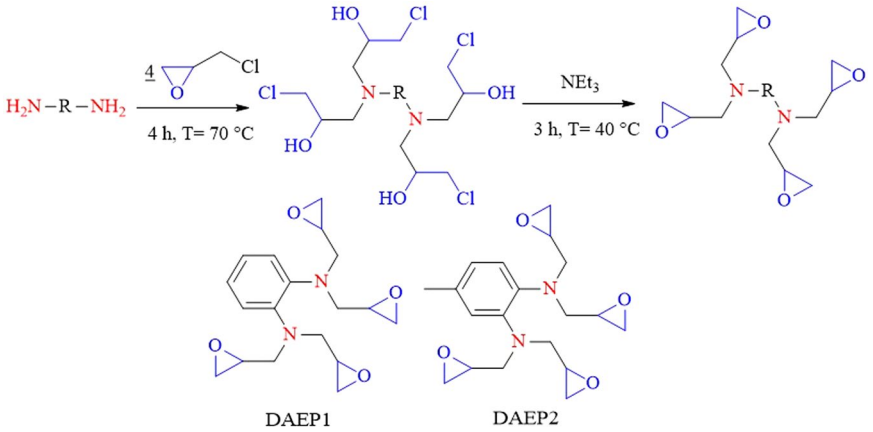

Figure 1. Schematic outline for the synthesis of two diamine aromatic epoxy pre-polymers DAEP1 and DAEP2.

different temperatures ranging from 20 to 80 °C. The dynamic rheology measurements (dynamic viscoelastic parameters such as the elastic G', G'' and η^*) as a function amplitude sweep 100–0.1 rad/s angular frequency were conducted at different temperatures ranging from 20–60 °C.

Electrochemical measurements. The electrochemical behavior of DAEPs was studied using Potentiostat (BioLogic SP-200 instrument as described in our earlier reports[26,27]. Stock solution of the inhibitors (DAEP1 and DAEP2) was prepared by dissolving them in small amount (nearly 2 mL) of isopropyl alcohol followed by the addition of tested electrolyte. Sample preparation and instrumental procedure for electrochemical studies was same as reported previously[26,27]. In order to get more accuracy and reproducibility of experimental data, the electrochemical studies were performed triply at each tested concentration of the DAEP1 and DAEP2 and mean values are reported. Inhibition effect of the DAEPswas evaluated using Eqs (1) and (2).

$$\eta_{EIS}\ \% = \frac{R_{ct} - R_{ct}^{0}}{R_{ct}} \times 100 \tag{1}$$

$$\eta_{\mathrm{PDP}}\ (\%) = \left(1 - \frac{i_{\mathrm{corr}}}{i_{\mathrm{corr}}^{0}}\right) \times 100 \tag{2}$$

where, R_{ct}^{0} and R_{ct} represent the charge transfer resistances values without and with DAEPs, respectively. Whereas, i^{0}_{corr} and i_{corr} are the current densities for steel corrosion without and with the DAEPs, respectively.

SEM characterization. For the surface study using SEM method, cleaned metallic specimens were allowed to dip and corrode for 12 h in 1 M HCl solution with and without DAEPs. After that metallic specimens were taken out bathed with sanitised water, and dried out in vacuity. The surfaces of the inhibited (by DAEPs) and uninhibited metallic specimens were inspected using a S3000H, Hitachi-Field Emission SEM instrument operated at 20 kV.

Computational details. For DFT study, both DAEP1 and DAEP2 were geometrically optimized using B3LYP/6-31 + G(d, p) level[28,29] in both gas phase and in aqueous solution as described elsewhere[30]. All calculations were performed using the G09 suite program[31]. Harmonic vibrational frequency study was employed to substantiate that all the structures obtained are read without imaginary functions (negative functions.) Since the experimental data were executed in acidic aqueous solution; the calculations accounted for solvent effect by applying. Visual inspections were performed using the GaussView program (version 5.0.8)[32] and Chemcraft program version 1.8 (build 489) (Chemcraft-graphical software for visualization of quantum chemistry computations were performed for the Visual inspections of the outputs.

Molecular dynamics simulations. MD simulations study was performed using Forcite module of Materials Studio 8.0 program developed by BIOVIA Inc. as described earlier[33–37]. A simulation box of 1.98 nm × 1.98 nm × 4.01 nm size consisting of periodic boundary conditions was selected for the simulations. The box consisted of a lower Fe slab and an upper solvent layer (containing 500 water molecules and one inhibitor molecule). For the iron substrate, Fe(110) was selected as explored surface since that it has a density packed structure and is the most stable. The Fe(110) exterior was modelled with a six-layer of 64 iron atoms in each *i. e.* (8 × 8) unit cell.

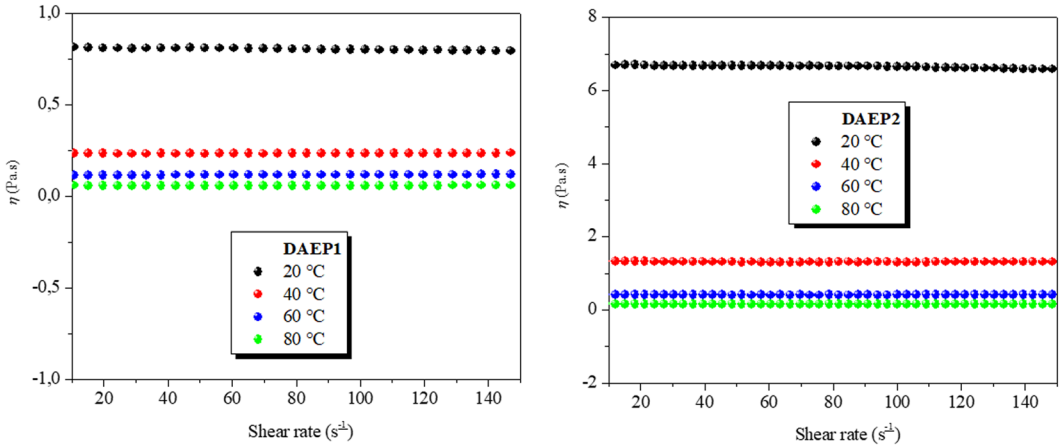

Figure 2. Viscosity measured as a function of shear for diamine aromatic epoxy pre-polymers DAEP1 and DAEP2 at different temperature.

Results and Discussion

Viscosity measurement. The viscosities of DAEPs were restrained as a purpose of shear rate at different temperatures range 20–80 °C as given in Fig. 2. The evolutions of the viscosity for diamine aromatic epoxy pre-polymers DAEP1 and DAEP2 with temperature permitted the estimation of the viscosity activation energy. The activation energy (E_a (kJ/mol)) of the diamine aromatic epoxy pre-polymers were calculated by Eq. (3) [38–40].

$$\eta(T) = \eta_0 \exp\left(\frac{E_a}{RT}\right) \tag{3}$$

where Viscosity (η) (Pa.s), η_0 is a constant, R the gas constant (8.314 j/mol.K) and T is temperature in K.

Arrhenius plots for the viscosity were given in Fig. SI3. Values of E_a for diamine aromatic epoxy pre-polymers were estimated by calculating the slope of Ln (η) vs. 1/T.

The activation energies for DAEP1 and DAEP2 are 38.36 kJmol^{-1} and 57.91 kJmol^{-1}, respectively. The results show that, the E_a for DAEP2 is higher than DAEP1 which can be attributed to the steric (electronic) repulsion between hydrophobic methyl (-CH_3) substituent and epoxy cycle. Availability of the -CH_3 in the molecular structure of DAEP2 enhances the bulkiness because of its high size as compared to the size of hydrogen of DAEP1. Apart from this, because of electron donating ability methyl substituent enhances the electron density over the aromatic ring which in turn affects the bulkiness of the entire molecule. It is important mention that the higher the activation energy value is related with higher viscosity[23].

Dynamic rheology measurements. The dynamic rheology studies were conducted for DAEP1 and DAEP2 and some dynamic rheological parameters, such as G', G'' and η^* derived at different temperatures. The dynamic rheological studies reveal the informations about the structures and dynamics of investigated system (DAEPs). Figure 3 shows the G' and G'' curves for the DAEPs. There is a well dependence of the dynamic modulus on the angular frequency as the G' and G'' increases with the increasing the angular frequency. Larson[41] illustrated that G' and G'' values give information about prototypical solid like and liquid-like materials/properties. Generally, Liquid-like behavior is expected for $G' < G''$ cases, whereas and solid-like behavior is expected for just inverse case ($G' > G''$). From the Fig. 3, we can see that for DAEP1, G' and G'' values are 46 Pa and 322 Pa, respectively, whereas for DAEP2G' and G'' values are 98 Pa and 345 Pa, respectively which suggests that DAEPs showed the property of a liquid-like at 20 °C ($G'' > G'$). However, careful inspection of the results showed that at 40 °C, for DAEP1, G' and G'' values are 745 Pa and 312 Pa, respectively, whereas for DAEP2 G' and G'' values are 876 Pa and 331 Pa, respectively. Whereas, at 60 °C, DAEP1, G' and G'' values are 1512 Pa and 226 Pa, respectively, whereas for DAEP2 G' and G'' values are 1661 Pa and 316 Pa, respectively. For temperatures between 40 and 60 °C, the elastic modulus (G'), which was higher in magnitude than the loss modulus (G'') for both DAEPs showed the property of a solid state ($G' > G''$). In order to avoid solid state property of the investigated molecules it is essential to store them at low temperature (T < 20 °C).

Figure 4 illustrates the complex viscosity (η^*) as function angular frequency for both studied DAEPs at different temperature (20, 40 and 60 °C). The dynamic viscosity reaches a constant value of 2.34 Pa.s for DAEP1 that was 3.41 Pa.s for DAEP2 at 20 °C. Complex viscosity is characteristic of a Newtonian fluid behavior for DAEPs. It is also clear from the figure that viscosity does not depend on the angular frequency at 20 °C. At 40 °C, the dynamic viscosities reach to 9.25 and 11.12 Pa.s for DAEP1 and DAEP2, respectively. At 60 °C, dynamic viscosities further increased to 16.91 Pa.s and 18.94 Pa.s for DAEP1 and DAEP2, respectively. It is also noticeable that dynamic viscosity is temperature-dependent phenomenon. The increase in the dynamic viscosities of DAEPs with increasing the angular frequency suggests that the DAEPs show non-Newtonian rheological behavior of pseudo plastic typeat temperatures 40 and 60 °C.

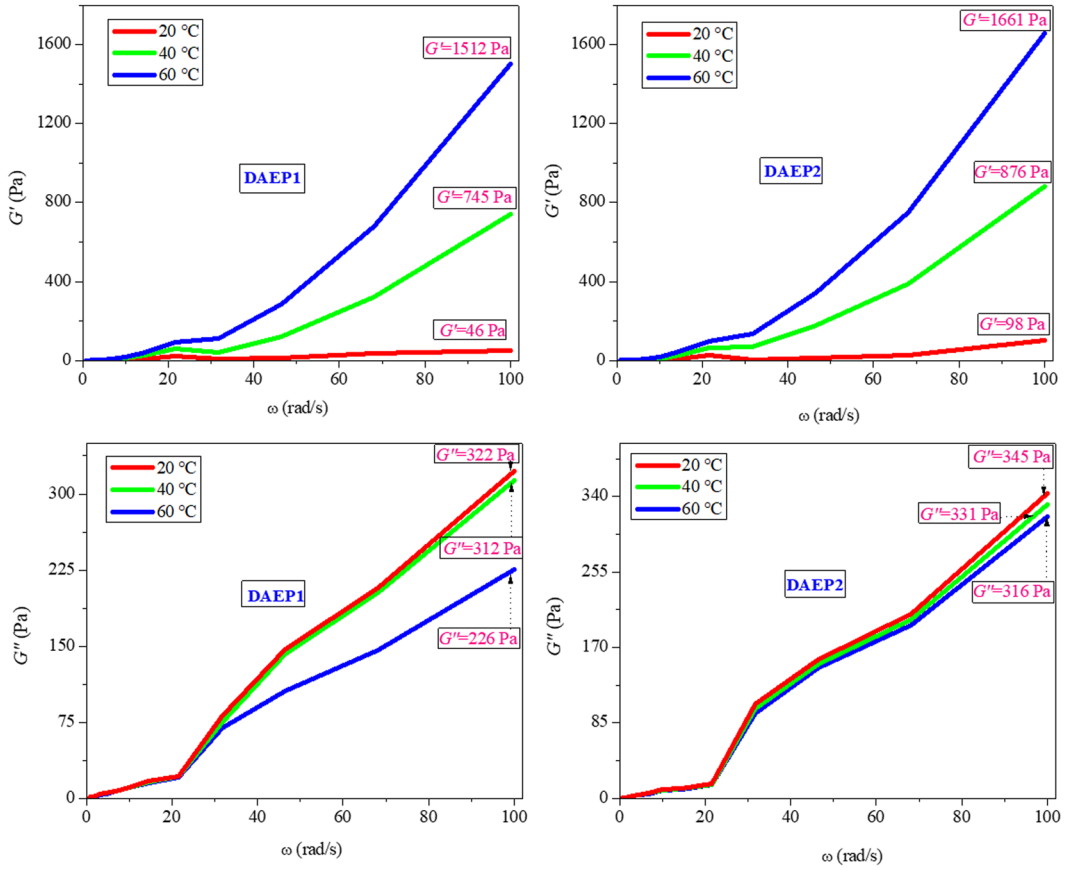

Figure 3. Changes of G' and G'' as functions of frequency for DAEP1 and DAEP2 at different temperatures.

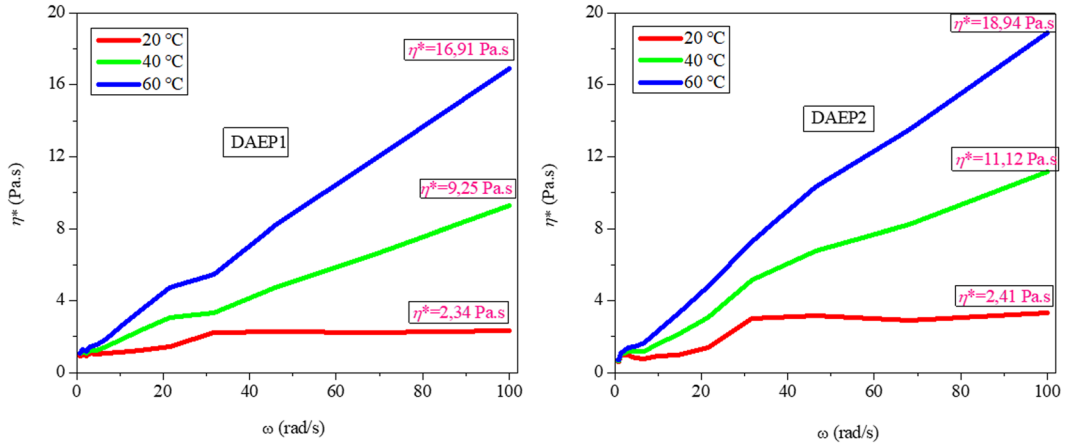

Figure 4. Changes complex viscosity as functions of frequency for DAEP1 and DAEP2 at different temperatures.

PDP study. The PDP curves for carbon steel dissolution without and with different concentrations of the DAEPs were measured to gather the information about kinetics of the anodic oxidative metallic dissolution and cathodic reductive hydrogen evolution.Fig. 5 shows the PDP curves without and with different concentrations of the diamine aromatic epoxy pre-polymers (DAEPs) and parameters are presented in Table 1.

The values (Table 1) of cathodic Tafel lines, β_c, show a slight change with increasing inhibitor concentration, indicating the influence of the DAEPs derivative on the kinetics of hydrogen evolution. This may probably be due to a diffusion or barrier effect. The values of the slopes of the anodic Tafel lines, β_a, was noticeably changed which proposes the role of inhibitors molecules adsorption on the active anodic sites on the iron dissolution mechanism. The anomalous behavior of anodic curves is related to the metal surface passivation as a result of inhibitor film deposition. It can also be noted that very little change in the values of E_{corr} of the inhibited Tafel curves were

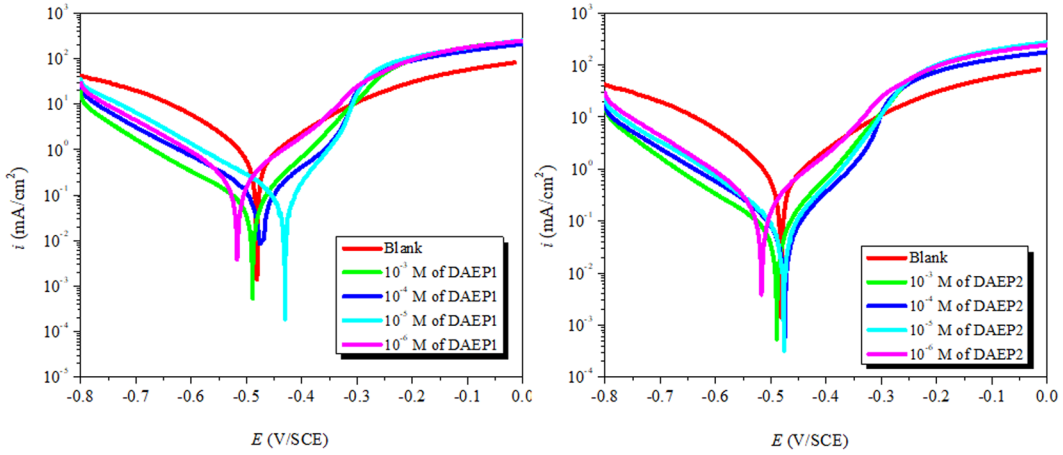

Figure 5. PDP curves for carbon steel corrosion in 1 M HCl solution in the absence and presence of different concentrations of DAEP1 and DAEP2.

Inh	C (M)	E_{corr} (mV/SCE)	i_{corr} (μA/cm²)	β_a (mV/dec)	$-\beta_c$ (mV/dec)	η%
Blank	—	−473.80	916.6 (±1.78)	163.6 (±1.10)	155.0 (±1.33)	—
DAEP1	10^{-3}	−489.32	075.40 (±0.36)	149.7 (±0.87)	151.3 (±1.79)	91.7
	10^{-4}	−473.58	133.67 (±0.57)	139.8 (±0.95)	168.7 (±1.68)	85.4
	10^{-5}	−429.96	172.98 (±0.85)	133.9 (±0.91)	168.2 (±1.67)	81.2
	10^{-6}	−516.72	250.88 (±0.93)	172.7 (±1.02)	177.6 (±1.71)	72.6
DAEP2	10^{-3}	−489.28	070.52 (±0.23)	084.9 (±0.65)	158.0 (±1.24)	92.3
	10^{-4}	−474.57	089.45 (±0.28)	067.7 (±0.42)	106.1 (±1.02)	90.0
	10^{-5}	−476.71	145.78 (±0.45)	136.8 (±0.89)	165.7 (±1.56)	84.0
	10^{-6}	−516.57	212.64 (±0.87)	111.4 (±0.77)	134.7 (±1.45)	76.8

Table 1. Potentiodynamic polarization parameters (±SD) for carbon steel corrosion in 1 M HCl solution in the absence and presence of different concentrations of DAEP1 and DAEP2.

observed with respect to the E_{corr} of black which suggests that DAEPs are mixed type corrosion inhibitors[42–44]. The inhibitory efficacies of the tested molecules followed the order: DAEP2 (92.3%) > DAEP1 (91.7%). The higher protectiveness of the DAEP2 as compared to DAEP1 can be attributed due to the presence of additional methyl substituent in the molecular structure of DAEP2 that enhances the electron density over the aromatic ring and thereby enhances the probability of the metal-inhibitor (DAEP2) interactions. The reasonably high inhibition effectiveness of the DAEP1 and DAEP2 can be attributed to the presence of several heteroatoms (N and O) that offer non-bonding electrons and aromatic rings that offer π-electrons for metal-inhibitor interactions. Apart from the metal-inhibitors (DAEPs) interactions, extensive presence of heteroatoms in the form of polar functional group(s) enhances the solubility of the investigated inhibitor molecules[6,23]. Results showed that DAEP 2 is a better corrosion inhibitor as compared to the DAEP1. It can be concluded that presence of methyl group (in DAPE2) can enhances the electron density over the active sites involving in the metal-inhibitor interactions. More so, after the adsorption of DAEP2 over the metallic surface, methyl group can enhance its protection efficiency by forming the hydrophobic surface film over the metallic surface. Therefore, methyl group can enhance the protection efficiency of DAEP2 as compared to the DAEP1 either by enhancing the electron density over the active sites because of its electron donating ability or by forming the hydrophobic surface films or by the combination of both.

EIS study. The Nyquistand Bode plots for carbon steel corrosion in 1 M HCl are presented in Fig. 6. It is easy to notice that Nyquist curves present a single capacitive loop over at frequency range from 10 mHz to 100 kHz, which is usually related to charge transfer phenomenon[45]. The capacitive plots are semicircles (imperfect circle), this is accredited to frequency spreading as a consequence of inhomogeneous behavior of electrode surface[46]. Increase in the diameter of semicircle on addition of DAEP1 and DAEP2 indicates that charge transfer phenomenon retorted or slow down due to adsorption of DAEPs at the interface of metal-electrolyte. Moreover, increase in diameter of the Nyquist plots is consistent with the concentration of DAEPs. Equivalent circuit model (shown in Fig. SI4) was used for fitting of Nyquist plots and calculation of EIS indices. The CPE is defined as the below Eq. (4) [47]:

$$Z_{CPE} = \frac{1}{Y_0(j\omega)^{\alpha}} \tag{4}$$

In the above equation, all symbols have their usual meaning[48]. The capacitance values (C_{dl}) is calculated using Eq. (5) [49,50]:

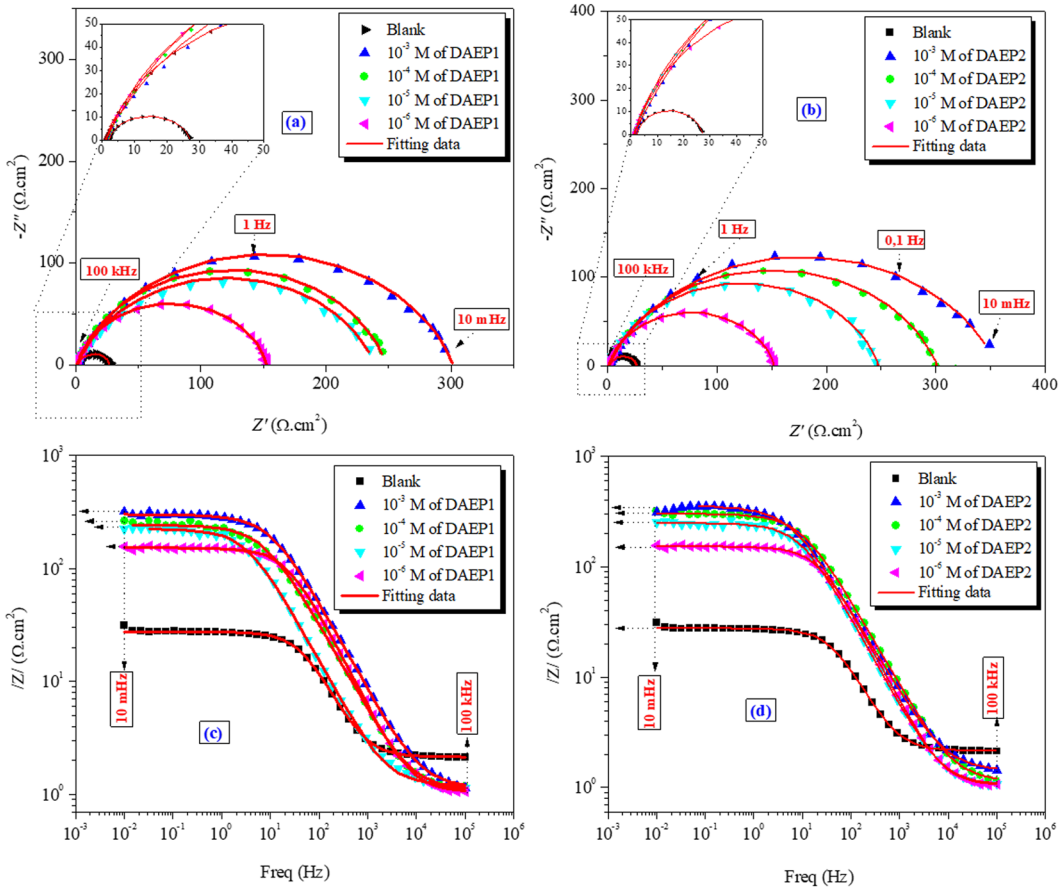

Figure 6. Nyquist and Bode diagrams for carbon steel in 1 M HCl solution in the absence and presence of different concentrations of DAEP1 and DAEP2.

Inh	C (M)	R_s (Ω. cm²)	R_{ct} (Ω. cm²)	C_{dl} (mF/cm²)	η%	χ^2
Blank	—	2.15 (±0.03)	25 (±1.52)	4.6 (±0.04)	—	0.056
DAEP1	10^{-3}	1.12 (±0.01)	300.4 (±3.36)	0.15 (±0.01)	91.7	0.109
	10^{-4}	1.07 (±0.01)	242.0 (±2.54)	0.18 (±0.02)	89.7	0.358
	10^{-5}	1.18 (±0.02)	224.0 (±2.32)	0.35 (±0.02)	88.8	0.251
	10^{-6}	1.04 (±0.03)	151.6 (±1.76)	0.96 (±0.03)	83.5	0.218
DAEP2	10^{-3}	1.41 (±0.02)	354.9 (±4.55)	0.17 (±0.01)	92.9	0.062
	10^{-4}	1.13 (±0.01)	300.4 (±3.23)	0.12 (±0.01)	91.6	0.109
	10^{-5}	1.05 (±0.03)	246.8 (±2.75)	0.14 (±0.02)	89.8	0.247
	10^{-6}	1.04 (±0.01)	151.1 (±1.96)	0.26 (±0.02)	83.4	0.274

Table 2. Electrochemical impedance spectroscopy parameters (±SD) for carbon steel corrosion in 1 M HCl solution in the absence and presence of different concentrations of DAEP1 and DAEP2.

$$C_{dl} = Y_0(\omega_{max})^{n-1} \quad (5)$$

As can be seen from Table 2, the R_{ct} values are enhancing with increasing the inhibitor concentration that can be ascribed to the formation of adsorption layer on the steel surface. The adsorbed inhibitors (DAEPs) films actas barrier for charge-transfer at the electrode surface. Similar to PDP results, EIS results showed that anticorrosive property of DAEP2 is relatively higher than inhibition property of DAEP1which clearly indicates that presence of electron releasing methyl group favor the metal-inhibitor(DAEPs) interactions[51]. Moreover, the C_{dl} values diminishon enhancing the concentration for the DAEPs. This results from the increase in the thickness of the protective layer and/or the decrease in local dielectric constant of the film[52].

Morphological analysis. The surface microstructure of the steel with the two diamine aromatic epoxy pre-polymers and in the absence of DAEP1 and DAEP2 was evaluated by SEM, and obtained micrographs are presented in Fig. 7(a–c). SEM observations taken after 12 h immersion time clearly show the difference between the three steel surfaces with and without DAEP1 and DAEP2. In Fig. 7a, the SEM micrograph for carbon steel

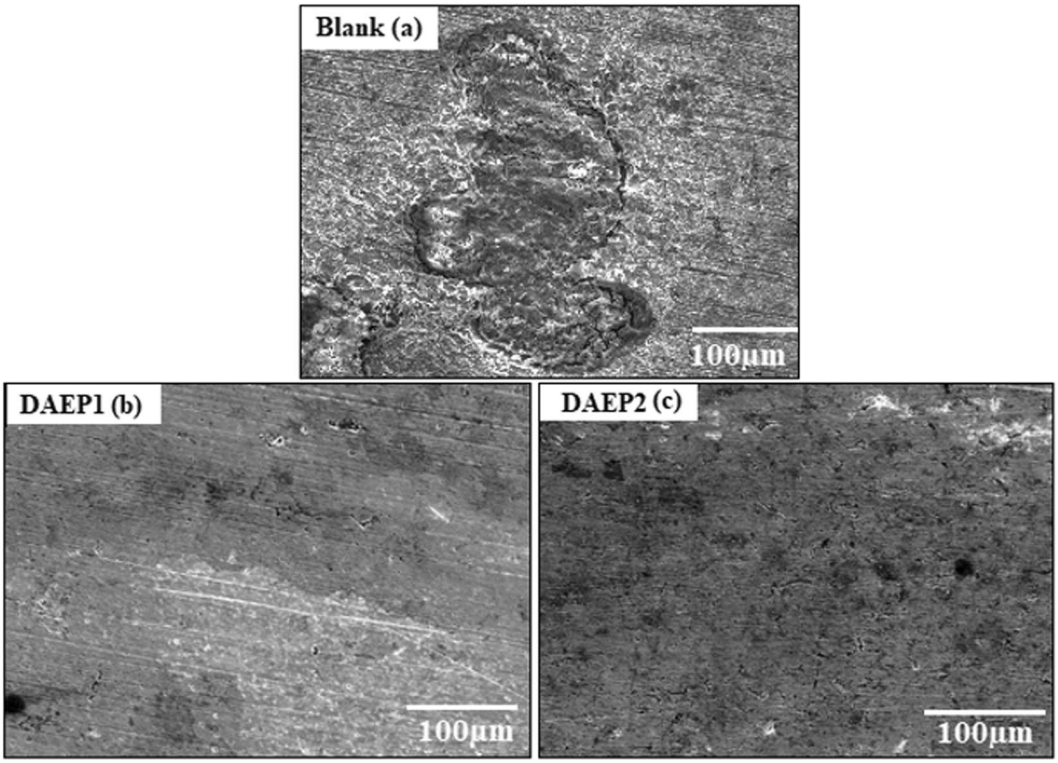

Figure 7. SEM micrographs of low carbon steel after 12 h of immersion in 1 M HCl solution: (**a**) without inhibitor, (**b**) and (**c**) with 10^{-3} M of DAEP1 and DAEP2, respectively.

after immersion in corrosive medium revealed that the metallic surface was damaged due to aggressive attack (from 1 M HCl solution), resulting in rapid corrosion. Figure 7b,c show the steel surface that was immersed for the same time interval in the acid solution containing 10^{-3} M concentration of DAEP1 and DAEP2, respectively. As can be seen, the surfaces damage has diminished due to the protective effects of DAEP1 (Fig. 7b) and DAEP2 (Fig. 7c), and particularly prominent in the case of the DAEP2 (Fig. 7c).

Adsorption studies. Metal-inhibitors (DAEPs) interactions can be most appropriately explained with the help of isotherm model. In present study, adsorption of the DAEP1 and DAEP2 obeyed the Langmuir isotherm model that can be presented as follows (6)[53].

$$\frac{C_{inh}}{\theta} = \frac{1}{K_{ads}} + C_{inh} \tag{6}$$

In above equation, all symbols have their usual meaning. Calculated values of K_{ads} were derived from intercept of the Langmuir isotherm model (i.e. C_{inh} and C_{inh}/θ) shown in Fig. SI5. Values of the ΔG_{ads} were calculated using Eq. (7) [54]:

$$K_{ads} = \frac{1}{55.5} exp\left(\frac{-\Delta G_{ads}}{RT}\right) \tag{7}$$

Generally, high positive value of K_{ads} and high negative value of ΔG_{ads} are associated with strong metal-inhibitor interactions[55,56]. The higher values of K_{ads} for DAEP2 indicate that it has stronger absorption ability than DAEP1 (Table SI3). The calculated ΔG_{ads} values for diamine aromatic epoxy pre-polymersis superior to −40 kJ/mol, indicating strongly interaction of DAEP1 and DAEP2 onto the metallic surface (Table SI3)[57]. Moreover, ΔG_{ads} values for diamine aromatic epoxy (DAEPs) of these pre-polymersmolecules decreases in the order ΔG_{ads} (DAEP2) > ΔG_{ads} (DAEP1).

Effect of temperature. PDP curves were recorded at different temperatures (298, 308, 318 and 328 K.) for carbon steel corrosion in 1 M HCl without and with DAEP1 and DAEP2 and derived results are presented in Fig. SI6. Results showed that protection efficiencyof DAEP1 and DAEP2 decreases on elevating the temperature (Table SI4). Therefore, increasing the temperature increases the corrosion current density from 75 to 923 µA. cm^{-2} for DAEP1, and from 70 to 501 µA. cm^{-2} for DAEP2, respectively. This result can be explaining by desorption of inhibitor molecules from carbon steel surface[6,23].

Theoretical studies. *Quantum chemical calculation.* To validate the experimental results and to gain a deeper insight into the reactivity of the studied DAEP1 and DAEP2 compounds, the calculated quantum global

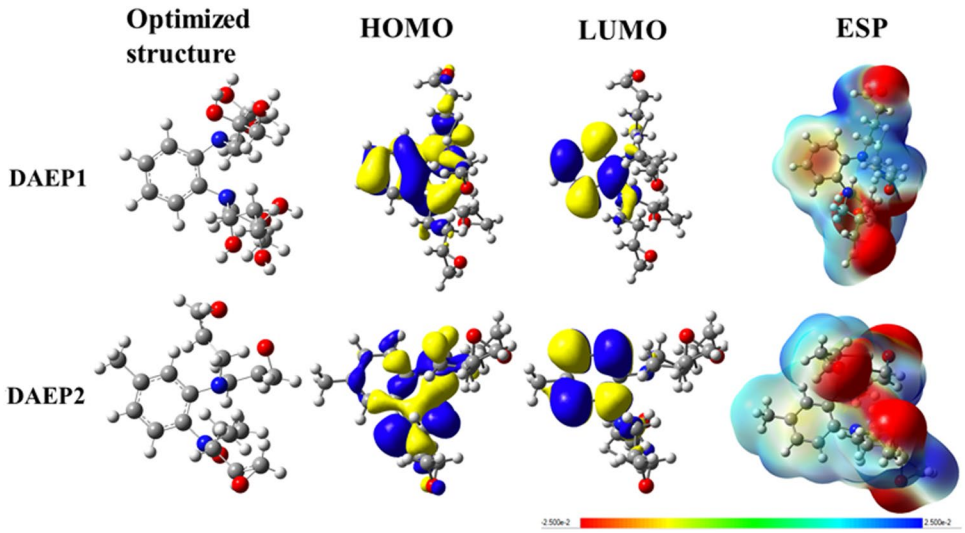

Figure 8. The optimized structures, HOMOs, LUMOs and ESP structures for theneutral inhibitor molecules using DFT/6-311 ++ G(d, p) calculation level in aqueous solution.

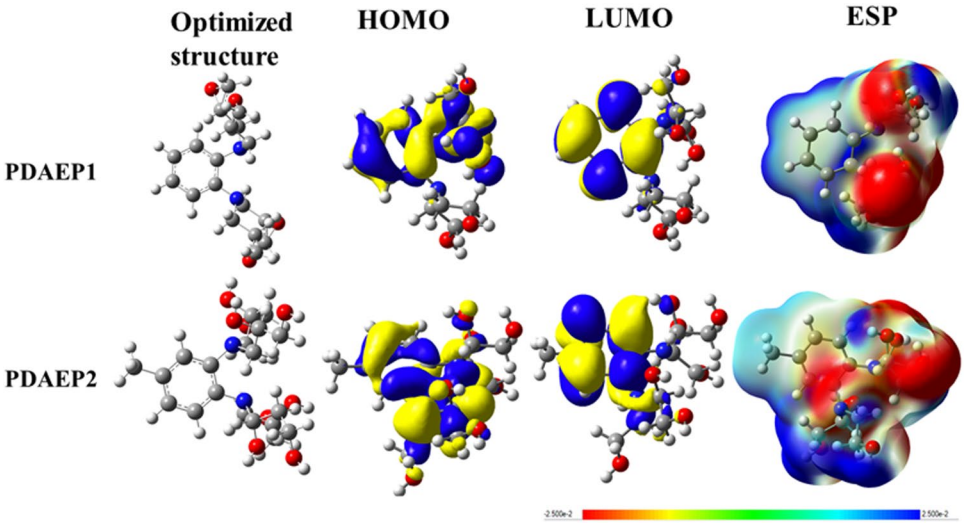

Figure 9. The optimized structures, HOMOs, LUMOs and ESP structures for the protonated inhibitor molecules using DFT/6-311 ++ G(**d, p**) calculation level in aqueous solution.

parameters, which were extracted based on the values of the highest occupied and lowest unoccupied molecular orbitals (E_{HOMO} and E_{LUMO}) were used. These parameters are the ionization potential ($I = -E_{HOMO}$), the electron affinity ($A = -E_{LUMO}$), the energy difference between E_{LUMO} and E_{HOMO}, ($\Delta E = (E_{HOMO} - E_{LUMO})$, the electronegativity ($\chi = (I + A)/2$) the global hardness ($\eta = (I - A)/2$) and softness ($\sigma = 1/\eta$), the fraction of electrons transferred ($\Delta N = (\varphi_{Fe} - \chi_{inh})/(2(\eta_{Fe} + \eta_{inh}))$, the electron transfer electron back-donation ($\Delta E_{back\text{-}donation} = -\eta/4$) and the initial molecule-metal interaction energy ($\Delta\psi = ((\chi_{Fe} - \chi_{inh})^2/(2(\eta_{Fe} + \eta_{inh}))$. It is important to mention that we selected work function(φ) is 4.82 eV for Fe (110) plan for the calculation of DFT parameters. The results are compiled in Table SI5, together with the total optimized energy (E)and the dipole moment (μ). Figures 8 and 9 show the optimized structures, the frontier molecular orbitals and electrostatic potential maps of the neutral and theprotonated species of the studied compound in aqueous solution, respectively. It was pointed out that the E_{HOMO} is frequentlyinterrelated with the electron donating propensity of the molecule into the vacant *d*-orbital of the metal, whereas, the E_{LUMO} corresponds to the electron acceptability of the inhibitor molecules from the vacant*d*-orbital of the metal surface[58–61]. The energy gap (ΔE) indicate the chemical reactivity of the inhibitorand its lower value associated with high efficiency[60–64].

As can be observed from Fig. 9, that HOMO is mainly localized over phenyl ring, the amino groups and the epoxy oxygen whereas LUMO density is localized exclusively on the methylene carbon atoms of the phenyl ring, indicating that this is these regions are mainly involving in electron(s) donation and acceptation, respectively during the metal-inhibitors interactions. The observation was also supported by ESP map.

As indicated in Table SI5, E_{HOMO}(DAEP2) > E_{HOMO} (DAEP1) in both gas phase and in aqueous solution. Similar trend is also seen for E_{LUMO} values, reflecting that DAEP2 moleculein its neutral form has the higher tendency to reactivity than DAEP1; this is not surprising considering that this inhibitor also has the higher tendency towards electron donation. Our obtained results show that the energy gap of DAEP2 in its neutral form is 0.105 and 0.113 eV smaller than that of the neutral DAEP2 in the gaps phase and aqueous solution, respectively. The solvent effect is clearly observing in decreasing of the energy gap of the studied species. Ongoing from gas phase to aqueous solution, our results show that the energy gap of DAEP2 decreases by 0.012 eV, which indicate that the DAEP2 compound is more reactive in aqueous solution than in the gas phase. The η and σ parameters are often correlated with the Pearson's hard and soft acids and bases (HSAB) and the Lewis theory of acid and bases[61–67]. Our obtained results in Table SI5 show that the η value of DAEP2 is smaller than that of the DAEP1 molecule, and therefore, the softness quantity of the DAEP1 inhibitor is smaller than the DAEP2 compound. Similar results are also observed in aqueous solution. Obot and Gasem[68] found that the compounds with the higher dipole moments are better inhibitors than those with lower dipole moments.

As indicated in Table SI5 that the dipole moment is aqueous solution of the DAEP2 is higher than the DAEP1, reflecting that the DAEP2 molecule is a more efficient inhibitor than the DAEP1 compound. It was pointed out as the number of electron transferred (ΔN)[68–70] to the vacant or partially vacant d-orbitals of the metal increases the inhibition efficiency of the molecule increases[60,61,68]. As can be seen in Table SI5, the ΔN(110) obtained for the DAEP2 molecule is 0.041 and 0.030 higher than that obtained for the DAEP1 molecule in the gas phase and solution respectively, which suggests that the inhibition efficiency of the DAEP2 molecule is higher than that of the DAEP1 one. In addition, the other tabulated parameters such as χ, $\Delta\psi$ and $\Delta E_{b\text{-}d}$ support our conclusions, which validate the experimental results described in the experimental section of this study.

The frontier electron distribution for protonated form of DAEPs is shown Fig. 9 and it can be seen that frontier electron (HOMO and LUMO) distribution is similar as was observed in the case of the neutral species. Comparison between the protonated and neutral species is as follows:

- The values of E_{HOMO} and E_{LUMO} of the protonated species are higher than the corresponding ones of the neutral species.
- The protonated species are softer and less hardness than the neutral inhibitors.
- The fraction of electrons transferred (ΔN) of the protonated species to the vacant orbitals of the metal surface is found to be higher than that of the neutral species.
- The electron transfer electron back-donation energy ($\Delta E_{back\text{-}donation}$) is higher for the protonated inhibitors compared to the neutral ones.
- The initial molecule-metal interaction energy ($\Delta\psi$) of the protonated inhibitors are higher than that of the neutral species.

As indicated in Table SI6 that the inhibition efficiency of the protonated inhibitors follows the order as: DAEP2 > DAEP1. Based on the above points, once can safely conclude that inhibition efficiency of the protonated species in aqueous solution is higher than in the gas phase.

MD simulation studies. The nature of meta-DAEPs interactions and orientations of DAEPs on metallic surface was further studied using MD simulation method. The equilibrium configurations (top and side view) of inhibitors adsorbed on the Fe (110) surface are shown in Fig. 10. As can be seen from Fig. 10 that the adsorption centers of both inhibitors on the Fe(110) surface are the electrons of benzene rings, oxygen and nitrogen heteroatoms. The inhibitor molecules epoxy pre-polymers DAEP1and DAEP2 adsorbed almost flat orientation on the iron surface to maximize surface coverage and contact, ensuring a strong interaction for adsorbate/substrate system. The adsorption energy (E_{ads}) for DAEPs adsorption can be calculated as follow (8):

$$E_{ads} = E_{total} - \left(E_{surf+water} + E_{inh+water}\right) + E_{water} \quad (8)$$

where E_{total} is denote the total energy related to metal-AEMs interactions, which include iron crystal, the adsorbed inhibitor molecule and solution; $E_{surf+water}$ and $E_{inh+water}$ are the potential energies of the system without the inhibitor and the system without the ironcrystal, respectively; E_{water} is the potential energy of the water molecules.

The obtained E_{ads} values are −834.1 and −853.3 kJ/mol for DAEP1 (a) and DAEP2 (b), respectively. Generally, the higher value of E_{ads} is consistent with the stronger the interaction between the inhibitors (DAEPs) and metal surface. Obviously, it appears that DAEP2 has a slightly higher absolute value of E_{ads} than DAEP1, and therefore it presents better inhibiting property for carbon steel, which is in consistent with the experimental findings.

The process of corrosion inhibition was highly influenced by the temperature. The equilibrium configurations of DAEP2 inhibitor adsorbed on the Fe(110) surface with different simulated temperatures were presented in Fig. 11. The obtained E_{ads} values are −853.3, −838.1, −780.5, and −754.7 kJ/mol at temperature 298 K, 308 K, 318 K and 328 K, respectively. From the results it can be observe that increase in the temperature causes significant decrease in the values of E_{ads} that can be resulted due to increase in the kinetic energy of the inhibitor molecules at elevated temperatures.

Conclusions

Two diamine aromatic epoxy pre-polymers (DAEPs) namely, N^1,N^1,N^2,N^2-tetrakis (oxiran-2-ylmethyl) benzene-1,2-diamine (DAEP1) and 4-methyl-N^1,N^1,N^2,N^2-tetrakis (oxiran-2-ylmethyl) benzene-1,2-diamine (DAEP2) were synthesized, characterized and evaluated as corrosion inhibitors in the corrosion of carbon steel in acidic medium.

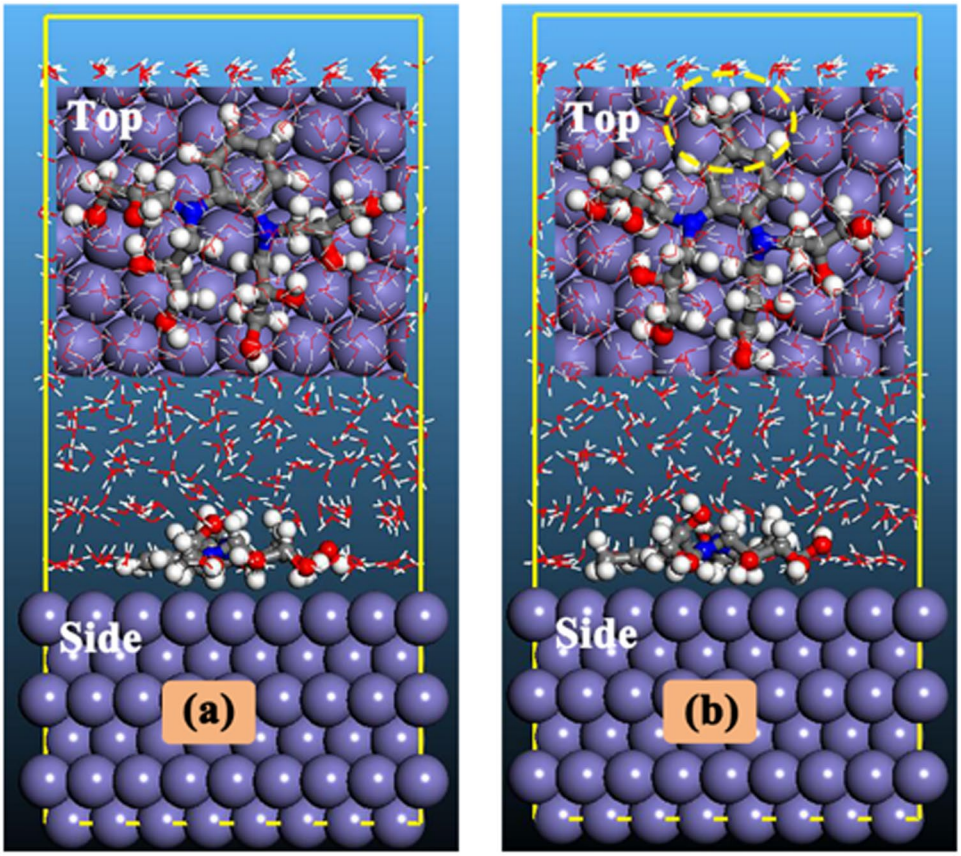

Figure 10. Side and top views of most stable adsorption configurations for (**a**) DAEP1 and (**b**) DAEP2 inhibitors on Fe(110) surface.

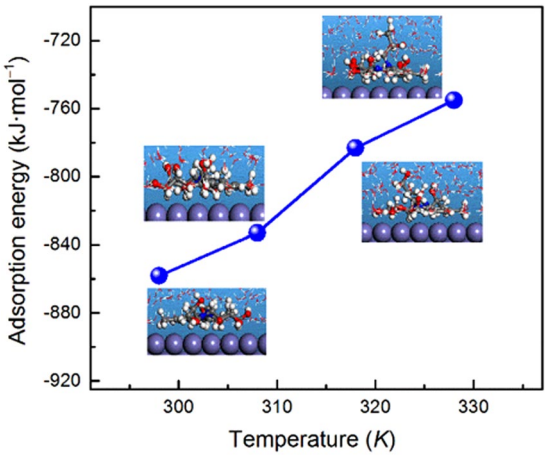

Figure 11. Dependence of adsorption energy on the temperature for adsorbed DAEP2 molecule on Fe(110).

From above experimental and theoretical studies, it can be concluded that:

1. Both DAEP1 and DAEP2 act as good corrosion inhibitors and their inhibition effectiveness is concentration, temperature and substituent dependent. Obviously, high inhibition effectiveness was observed at low temperature, high inhibitor (DAEPs) concentration and electron releasing methyl substituent.
2. The highest inhibition efficiency values at 10^{-3} M (optimum concentration) are 91.7% and 92.9% for DAEP1 and DAEP2, respectively.

1. The PDP results reveal that, the diamine aromatic epoxy pre-polymers(DAEPs) behave as mixed type inhibitors.
2. EIS studies revealed the adsorption of DAEPs molecules and are confirmed by increase in R_{ct} and decrease in C_{dl} values, respectively.
3. Adsorption of the tested diamine aromatic epoxy pre-polymersmolecules obeyed Langmuir adsorption isotherm.
4. Very high negative magnitude of the ΔG_{ads} (−44.42 to −45.58 kJ/mol) values showed that DAEP1 and DAEP2 interact spontaneously and strongly with the metallic surface.
5. Theoretical results of the neutral and protonated species in both gas phase and aqueous solution indicated that the DAEP2 inhibitor is more efficient than DAEP1 one, which is completely agree with the experimental results.
6. The more negative value of E_{ads} for DAEP2 as compared to the DAEP1 indicates that later case has relatively strong probability of meta-inhibitor interactions as compared to former one.

References

1. Lin, B. & Zuo, Y. Corrosion inhibition of carboxylate inhibitors with different alkylene chain lengths on carbon steel in an alkaline solution. *RSC Adv.* **9**(13), 7065–7077 (2019).
2. Haque, J. *et al*. N-trioctylammonium chloride as a novel and green corrosion inhibitor for mild steel in an acid chloride medium: electrochemical, DFT and MD. *studies. N. J. Chem*. **41**(22), 13647–13662 (2017).
3. El Faydy, M. *et al*. Corrosion inhibition performance of newly synthesized 5-alkoxymethyl-8-hydroxyquinoline derivatives for carbon steel in 1 M HCl solution: experimental, DFT and Monte Carlo simulation studies. *Phys. Chem. Chem. Phys.* **20**(30), 20167–20187 (2018).
4. Sukul, D. *et al*. Newly synthesized quercetin derivatives as corrosion inhibitors for mild steel in 1 M HCl: combined experimental and theoretical investigation. *Phys. Chem. Chem. Phys*. **20**(9), 6562–6574 (2018).
5. Sliem, M. H. *et al*. AEO7 Surfactant as an Eco-Friendly Corrosion Inhibitor for Carbon Steel in HCl solution. *Scientific reports*. **9**(1), 2319 (2019).
6. Dagdag, O. *et al*. Adsorption and anticorrosive behavior of aromatic epoxy monomers on carbon steel corrosion in acidic solution: computational studies and sustained experimental studies. *RSC Adv.* **9**(26), 14782–14796 (2019).
7. Al-Amiery, A. A., Kassim, F. A. B., Kadhum, A. A. H. & Mohamad, A. B. Synthesis and characterization of a novel eco-friendly corrosion inhibition for mild steel in 1 M hydrochloric acid. *Scientific reports*. **6**, 19890 (2016).
8. Verma, C., Quraishi, M. A., Olasunkanmi, L. O. & Ebenso, E. E. L-Proline-promoted synthesis of 2-amino-4-arylquinoline-3-carbonitriles as sustainable corrosion inhibitors for mild steel in 1 M HCl: experimental and computational studies. *RSC Adv.* **5**(104), 85417–85430 (2015).
9. Baig, N., Chauhan, D. S., Saleh, T. A. & Quraishi, M. A. Diethylenetriamine functionalized graphene oxide as a novel corrosion inhibitor for mild steel in hydrochloric acid solutions. *N. J. Chem*. **43**(5), 2328–2337 (2019).
10. Verma, C., Sorour, A. A., Ebenso, E. E. & Quraishi, M. A. Inhibition performance of three naphthyridine derivatives for mild steel corrosion in 1M HCl: Computation and experimental analyses. *Res. Phys.* **10**, 504–511 (2018).
11. Zhang, W. *et al*. Highly effective inhibition of mild steel corrosion in HCl solution by using pyrido [1, 2-a] benzimidazoles. *N. J. Chem*. **43**(1), 413–426 (2019).
12. Dagdag, O. *et al*. Anticorrosive properties of Hexa (3-methoxy propan-1, 2-diol) cyclotri-phosphazene compound for carbon steel in 3% NaCl medium: gravimetric, electrochemical, DFT and Monte Carlo simulation studies. *Heliyon*. **5**(3), e01340 (2019).
13. Singh, A. *et al*. Effect of electron donating functional groups on corrosion inhibition of mild steel in hydrochloric acid: Experimental and quantum chemical study. *J. Tai. Inst. Chem. Eng*. **82**, 233–251 (2018).
14. Dohare, P., Ansari, K. R., Quraishi, M. A. & Obot, I. B. Pyranpyrazole derivatives as novel corrosion inhibitors for mild steel useful for industrial pickling process: experimental and quantum chemical study. *J. Indus. Eng. Chem*. **52**, 197–210 (2017).
15. El-Haddad, M. A., Radwan, A. B., Sliem, M. H., Hassan, W. M. & Abdullah, A. M. Highly efficient eco-friendly corrosion inhibitor for mild steel in 5 M HCl at elevated temperatures: experimental & molecular dynamics study. *Scientific reports*. **9**(1), 3695 (2019).
16. Dagdag, O. *et al*. Polymeric-Based Epoxy Cured with a Polyaminoamide as an Anticorrosive Coating for Aluminum 2024-T3 Surface: Experimental Studies Supported by Computational Modeling. *J. Bio. Tri. Corros.* **5**(3), 58 (2019).
17. Saha, S. K., Dutta, A., Ghosh, P., Sukul, D. & Banerjee, P. Adsorption and corrosion inhibition effect of Schiff base molecules on the mild steel surface in 1 M HCl medium: a combined experimental and theoretical approach. *Phys. Chem. Chem. Phys.* **17**(8), 5679–5690 (2015).
18. Dagdag, O., Hamed, O., Erramli, H. & El Harfi, A. Anticorrosive Performance Approach Combining an Epoxy Polyaminoamide–Zinc Phosphate Coatings Applied on Sulfo-tartaric Anodized Aluminum Alloy 5086. *J. Bio. Tribo. Corros.* **4**(4), 52 (2018).
19. Dagdag, O., *et al* Synthesis, characterization and rheological properties of epoxy monomers derived from bifunctional aromatic amines. *Poly. Bull*. 1–15 (2018).
20. Dagdag, O. *et al*. Anticorrosive Performance of New Epoxy-Amine Coatings Based on Zinc Phosphate Tetrahydrate as a Nontoxic Pigment for Carbon Steel in NaCl Medium. *Arab. J. Sci Eng.* **43**(11), 5977–5987 (2018).
21. Dagdag, O. *et al*. Phosphorous-based epoxy resin composition as an effective anticorrosive coating for steel. *Inter. J. Indus. Chem*. **9**(3), 231–240 (2018).
22. Dagdag, O. *et al*. Electrochemical impedance spectroscopy (SIE) evaluation of the effect of immersion time of the protective matrix based on a polymer Tetra Glycidyl of Ethylene Dianiline (TGEDA) on carbon steel in 3% NaCl. *Inter. J. ChemTech Res*. **9**(04), 390–399 (2016).
23. Dagdag, O. *et al*. Rheological, electrochemical, surface, DFT and molecular dynamics simulation studies on the anticorrosive properties of new epoxy monomer compound for steel in 1 M HCl solution. *RSC Adv*. **9**(8), 4454–4462 (2019).
24. Dagdag, O. Theoretical studies of cyclophosphazene derivative as corrosion inhibitor for carbon steel in sodium chloride. *Der Phar. Chem*. **7**, 46–54 (2015).
25. Dagdag, O., *et al* Application of hexa propylene glycol cyclotriphosphazene as corrosion inhibitor for copper in 3% NaCl solution. *Der Phar. Chem*. **7(4)** (2015).
26. Dagdag, O. *et al*. The role of zinc phosphate pigment in the anticorrosion properties of bisphenol A diglycidyl ether-polyaminoamide coating for aluminum alloy AA2024-T3. *J. Bio. Tribo. Corros.* **5**(1), 7 (2019).
27. Dagdag, O., El Gana, L., Hamed, O., Jodeh, S. & El Harfi, A. Anticorrosive Formulation Based of the Epoxy Resin–Polyaminoamide Containing Zinc Phosphate Inhibitive Pigment Applied on Sulfo-Tartaric Anodized AA 7075-T6 in NaCl Medium. *J. Bio. Tribo. Corros.* **5**(1), 25 (2019).
28. Becke, A. D. Density-functional exchange-energy approximation with correct asymptotic behavior. *Phys. review A*. **38**(6), 3098 (1988).

29. Lee, C., Yang, W. & Parr, R. G. Development of the Colle-Salvetti correlation-energy formula into a functional of the electron density. *Physical review B* **37**(2), 785 (1988).
30. Barone, V. & Cossi, M. Quantum calculation of molecular energies and energy gradients in solution by a conductor solvent model. *J. Phys. Chem. A.* **102**(11), 1995–2001 (1998).
31. Frisch, M. J. E. A., *et al* Gaussian 09. revision D. 01 (2009).
32. Dennington, R., Keith, T. & Millam, J. GaussView, version 5. *Semichem Inc.: Shawnee Mission. KS* (2009).
33. Tan, B. *et al*. Corrosion inhibition of X65 steel in sulfuric acid by two food flavorants 2-isobutylthiazole and 1-(1, 3-Thiazol-2-yl) ethanone as the green environmental corrosion inhibitors: Combination of experimental and theoretical researches. *J. Col. Inter. Sci.* **538**, 519–529 (2018).
34. El Bakri, Y., Guo, L. & Essassi, E. M. Electrochemical, DFT and MD simulation of newly synthesized triazolotriazepine derivatives as corrosion inhibitors for carbon steel in 1 M HCl. *J. Mol. Liq.* **274**, 759–769 (2019).
35. Saha, S. K., Dutta, A., Ghosh, P., Sukul, D. & Banerjee, P. Novel Schiff-base molecules as efficient corrosion inhibitors for mild steel surface in 1 M HCl medium: experimental and theoretical approach. *Phys. Chem. Chem. Phys.* **18**(27), 17898–17911 (2016).
36. El Bakri, Y. *et al*. Synthesis, crystal structure, DFT, molecular dynamics simulation and evaluation of the anticorrosion performance of a new pyrazolotriazole derivative. *J. Mol. Struct.* **1176**, 290–297 (2019).
37. Saha, S. K., Dutta, A., Ghosh, P., Sukul, D. & Banerjee, P. Adsorption and corrosion inhibition effect of Schiff base molecules on the mild steel surface in 1 M HCl medium: a combined experimental and theoretical approach. *Phys. Chem. Chem. Phys.* **17**(8), 5679–5690 (2015).
38. El Hamdaoui, L., El Bouchti, M. & El Moussaouiti, M. Comparison of rheological properties of kraft and microcrystalline cellulose dissolved in lithium chloride/N, N-dimethylacetamide. *Poly. Bul.* **75**(2), 769–779 (2018).
39. Al-Omair, N. A. *et al*. A partial derivatives approach for estimation of the viscosity Arrhenius temperature in N, N-dimethylformamide+ 1, 4-dioxane binary fluid mixtures at temperatures from 298.15 K to 318.15 K. *Phys. Chem. Liq.* **54**(5), 615–631 (2016).
40. Dallel, M. *et al*. Prediction of the boiling temperature of 1, 2-dimethoxyethane and propylene carbonate through the study of viscosity–temperature dependence of corresponding binary liquid mixtures. *Phys. Chem. Liq.* **55**(4), 541–557 (2017).
41. Hao, Y. *et al*. Effect of epoxy resin on the thermal, mechanical and rheological properties of polybutylene terephthalate/glycidyl methacrylate functionalized methyl methacrylate-butadiene blend. *Chem. Res Chin. Uni.* **32**(1), 140–148 (2016).
42. Verma, C., Quraishi, M. A., Ebenso, E. E., Obot, I. B. & El Assyry, A. 3-Amino alkylated indoles as corrosion inhibitors for mild steel in 1M HCl: Experimental and theoretical studies. *J. Mol. Liq.* **219**, 647–660 (2016).
43. Heydari, H. *et al*. Comparison of two Schiff bases containing O-methyl and nitro substitutes for corrosion inhibiting of mild steel in 1 M HCl solution. *J. Mol. Liq.* **254**, 177–187 (2018).
44. Solomon, M. M., Umoren, S. A., Quraishi, M. A. & Mazumder, M. J. Corrosion inhibition of N80 steel in simulated acidizing environment by N-(2-(2-pentadecyl-4, 5-dihydro-1H-imidazol-1-YL) ethyl) palmitamide. *J. Mol. Liq.* **273**, 476–487 (2019).
45. Murmu, M., Saha, S. K., Murmu, N. C. & Banerjee, P. Effect of stereochemical conformation into the corrosion inhibitive behaviour of double azomethine based Schiff bases on mild steel surface in 1 mol L^{-1} HCl medium: An experimental, density functional theory and molecular dynamics simulation study. *Corros. Sci.* **146**, 134–151 (2019).
46. Sebhaoui, J. *et al*. Synthesis, NMR characterization, DFTand anti-corrosion on carbon steel in 1M HCl of two novel 1, 5-benzodiazepines. *J. Mol. Struct.* **1182**, 123–130 (2019).
47. Liang, C. *et al*. Synthesis of 2-aminofluorene bis-Schiff base and corrosion inhibition performance for carbon steel in HCl. *J. Mol. Liq.* **277**, 330–340 (2019).
48. Badr, E. A., Bedair, M. A. & Shaban, S. M. Adsorption and performance assessment of some imine derivatives as mild steel corrosion inhibitors in 1.0 M HCl solution by chemical, electrochemical and computational methods. *Mat. Chem. Phys.* **219**, 444–460 (2018).
49. El-Hajjaji, F. *et al*. Effect of 1-(3-phenoxypropyl) pyridazin-1-ium bromide on steel corrosion inhibition in acidic medium. *J. Col. Inter. Sci.* **541**, 418–424 (2019).
50. Sanaei, Z., Ramezanzadeh, M., Bahlakeh, G. & Ramezanzadeh, B. Use of Rosa canina fruit extract as a green corrosion inhibitor for mild steel in 1 M HCl solution: A complementary experimental, molecular dynamics and quantum mechanics investigation. *J. Indus. Eng. Chem.* **69**, 18–31 (2019).
51. Ramya, K., Mohan, R. & Joseph, A. Interaction of benzimidazoles and benzotriazole: its corrosion protection properties on mild steel in hydrochloric acid. *J. Mat. Eng. Perf.* **23**(11), 4089–4101 (2014).
52. El-Lateef, H. M. A., Adam, M. S. S. & Khalaf, M. M. Synthesis of polar unique 3d metal-imine complexes of salicylidene anthranilate sodium salt. *Homogeneous catalytic and corrosion inhibition performance. J. Tai. Ins. Chem. Eng.* **88**, 286–304 (2018).
53. Mobin, M., Basik, M. & Shoeb, M. A novel organic-inorganic hybrid complex based on Cissus quadrangularis plant extract and zirconium acetate as a green inhibitor for mild steel in 1 M HCl solution. *Appl. Surf. Sci.* **469**, 387–403 (2019).
54. Cui, M., Ren, S., Zhao, H., Wang, L. & Xue, Q. Novel nitrogen doped carbon dots for corrosion inhibition of carbon steel in 1 M HCl solution. *Appl. Surf. Sci.* **443**, 145–156 (2018).
55. Aoun, S. B. On the corrosion inhibition of carbon steel in 1 M HCl with a pyridinium-ionic liquid: chemical, thermodynamic, kinetic and electrochemical studies. *RSC Adv.* **7**(58), 36688–36696 (2017).
56. Espinoza-Vázquez, A. *et al*. Synthesis of 1, 2, 3-triazoles in the presence of mixed Mg/Fe oxides and their evaluation as corrosion inhibitors of API 5L X70 steel submerged in HCl. *RSC Adv.* **7**(40), 24736–24746 (2017).
57. Dagdag, O., *et al* Anticorrosive property of heterocyclic based epoxy resins on carbon steel corrosion in acidic medium: Electrochemical, surface morphology, DFT and Monte Carlo simulation studies. *J. Mol. Liq.* 110977 (2019).
58. Mihit, M. *et al*. Study of the inhibition of the corrosion of copper and zinc in HNO_3 solution by electrochemical technique and quantum chemical calculations. *Arab. J. Chem.* **3**(1), 55–60 (2010).
59. Saha, S. K., Ghosh, P., Hens, A., Murmu, N. C. & Banerjee, P. Density functional theory and molecular dynamics simulation study on corrosion inhibition performance of mild steel by mercapto-quinoline Schiff base corrosion inhibitor. *Phys. E: L.dimens. Syst. Nanostr.* **66**, 332–341 (2015).
60. Erdoğan, Ş. *et al*. A computational study on corrosion inhibition performances of novel quinoline derivatives against the corrosion of iron. *J. Mol. Struct.* **1134**, 751–761 (2017).
61. Guo, L. *et al*. Anticorrosive effects of some thiophene derivatives against the corrosion of iron: A computational study. *Front. Chem.* **6**, 155 (2018).
62. Hammouti, B., Dafali, A., Touzani, R. & Bouachrine, M. Inhibition of copper corrosion by bipyrazole compound in aerated 3% NaCl. *J. S. Chem. Soc.* **16**(4), 413–418 (2012).
63. Zhang, F. *et al*. Performance and theoretical study on corrosion inhibition of 2-(4-pyridyl)-benzimidazole for mild steel in hydrochloric acid. *Corros. Sci.* **61**, 1–9 (2012).
64. Yadav, M., Sinha, R. R., Kumar, S., Bahadur, I. & Ebenso, E. E. Synthesis and application of new acetohydrazide derivatives as a corrosion inhibition of mild steel in acidic medium: Insight from electrochemical and theoretical studies. *J. Mol. Liq.* **208**, 322–332 (2015).
65. Pearson, R. G. Absolute electronegativity and hardness correlated with molecular orbital theory. *Proceed. Nat. Acad. Sci.* **83**(22), 8440–8441 (1986).
66. Dagdag, O. *et al*. Rheological, electrochemical, surface, DFT and molecular dynamics simulation studies on the anticorrosive properties of new epoxy monomer compound for steel in 1 M HCl solution. *RSC Adv.* **9**(8), 4454–4462 (2019).

67. Martinez, S. Inhibitory mechanism of mimosa tannin using molecular modeling and substitutional adsorption isotherms. *Mat. Chem. Phys.* **77**(1), 97–102 (2003).
68. Obot, I. B. & Gasem, Z. M. Theoretical evaluation of corrosion inhibition performance of some pyrazine derivatives. *Corros. Sci.* **83**, 359–366 (2014).
69. Olasunkanmi, L. O., Obot, I. B. & Ebenso, E. E. Adsorption and corrosion inhibition properties of N-{n-[1-R-5-(quinoxalin-6-yl)−4, 5-dihydropyrazol-3-yl] phenyl} methanesulfonamides on mild steel in 1 M HCl: experimental and theoretical studies. *RSC Adv.* **6**(90), 86782–86797 (2016).
70. Singh, P., Ebenso, E. E., Olasunkanmi, L. O., Obot, I. B. & Quraishi, M. A. Electrochemical, theoretical, and surface morphological studies of corrosion inhibition effect of green naphthyridine derivatives on mild steel in hydrochloric acid. *J. Phys. Chem. C.* **120**(6), 3408–3419 (2016).

Acknowledgements

C.V. thankfully acknowledges the North-West University (Mafikeng Campus) for financial support under postdoc fellowship scheme. Nuha Wazzan gratefully acknowledges King Abdulaziz University's High Performance Computing Centre (Aziz Supercomputer) (http://hpc.kau.edu.sa) for assisting with the calculations for this study. This research was partially supported by the National Natural Science Foundation of China (21706195), the Science and Technology Program of Guizhou Province (QKHJC2016-1149), and the Guizhou Provincial Department of Education Foundation (QJHKYZ2016-105).

Author Contributions

O. Dagdag, R. Hsissou, H. Erramli and M.E. Bouchti carried out the experimental works. Z. Safi, N. Wazzan and L. Guo completed the computational studies. C. Verma, E.E. Ebenso and A. E. Harfi conceptualized and designed the work and were part of the manuscript writ-up.

Additional Information

Supplementary information accompanies this paper at https://doi.org/10.1038/s41598-019-48284-0.

Competing Interests: The authors declare no competing interests.

Publisher's note: Springer Nature remains neutral with regard to jurisdictional claims in published maps and institutional affiliations.